A98-31542

ICAS-98-3,3,4

CAPABILITIES OF SURFACE MEASUREMENT TECHNIQUES AND THEIR IMPACT ON MODERN WING-DESIGN AND ASSESSMENT

W. Nitsche, S. Bose, F. Haselbach, J. Suttan
Institut für Luft- und Raumfahrt, Technische Universität Berlin, Marchstr. 12-14
Sekretariat F2, 10587 Berlin, Germany

Abstract

Steady and unsteady surface measurement techniques for subsonic and transonic flows are surveyed emphasizing their capabilities on modern wing design and assessment. In this context, the present paper first investigates the accuracy of some existing sensor techniques for the determination of the mean wall shear stress (Preston Tube (CPM3), Surface Hot-Film, Obstacle Wire) in transonic flows, using a floating element balance as a reference. Additionally, the status and the capabilities of a number of improved surface measurement techniques (Surface Hot-Film Array, Piezo-Array, Liquid Crystals), which are necessary for the analysis of distributed flow phenomena on airfoils, like boundary layer (b.l.) transition, shock b.l. interaction or separation, are demonstrated in wind tunnel as well as in in-flight tests. By this, different test cases are comparatively investigated using the mentioned techniques, in order to evaluate their capabilities for monitoring the boundary layer state on airfoils.

Nomenclature

A,B	calibration constant [-]
A^+	van Driest constant [-]
c	chord length [m]
d	diameter [m]
f_E	excitation frequency [Hz]
K_1	von Karman constant [-]
L,l,s	length [m]
M	Mach number [-]
N_s	number of sensors [-]
p	pressure [Pa]
p^+	non dim. pressure gradient [-]
dp/dx	pressure gradient [Pa/m]
Q	electrical charge [C]
Q_{el}	electrical heat loss [J/s]
r	radius [m]
Re	Reynolds number [-]
S	spacing of sensors [m]
T	temperature [K]
u	velocity [m/s]
U	voltage [V]
x,y	coordinates [m]
y	wall distance [m]
α	angle of attack [°]
λ	thermal conductivity [J/msK]
δ	b.l. thickness [m]
ρ	density [kg/m^2]
μ	dyn. viscosity [Ns/m^2]
τ_w	skin friction [N/m^2]
ν	kin. viscosity [m^2/s]

Index

hf	hot-film
ow	obstacle wire
eff	effective
f	fluid
s	sensor
w	wall
Δ	differential
ref	reference
+	non-dimensional
∞	free stream

Introduction

The analysis of the efficiency of an improved wing design for future aircraft requires - in addition to the knowledge of the basic aerodynamic performance obtained by pressure and force measurements - a sufficient and reliable data base - provided by surface measurement techniques - in order to analyse the b.l. relevant phenomena[1][2]. For example, in the scope of hybrid laminar wings and/or adaptive wings for future transport aircraft, reliable measurement techniques are needed for the monitoring of wall bounded shear flows in order to verify the capabilities of a new wing design in wind tunnel pre-tests as well as during service. By means of these measurement techniques, a verification and control of the impact of the specific active and/or passive flow control devices should be provided.

Such investigations are of great relevance when analysing local and/or distributed flow phenomena, such as laminar-turbulent transition, shock-boundary layer interaction and shock or pressure induced separation. Thus, surface measurement

21st ICAS Congress
13-18 September 1998
Melbourne, Australia

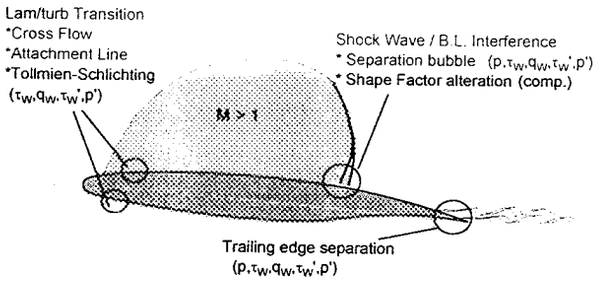

Figure 1: Local flow phenomena on a transonic wing section and correlated quantities at the wall (schematic sketch)

techniques should be capable of both, high spatial and temporal resolution, delivering data for the understanding and control of relevant phenomena in the transonic flow regime. Fig. 1 gives an overview of some possible flow phenomena on a transonic wing section and the correlated measurement quantities. In this framework, the paper first surveys the capabilities of existing measurement techniques for the determination of the mean wall shear stress (Preston Tube and Computational Preston Tube (CPM3), Surface Hot-Film, Obstacle Wire) in order to detect these flow phenomena.

These non(less)-intrusive measurement techniques may be used for calibration of the multi-sensor measurement techniques or as simple qualitative/quantitative measurement devices providing an information about successful or unsuccessful laminarisation (yes/no-statement).

Additionally, the paper investigates comparatively the status and capabilities of a number of improved surface measurement techniques (Hot-Film-Arrays, Piezo-Arrays, Liquid Crystals) which are necessary for the understanding of distributed flow phenomena like transition and separation.

The comparative survey presented in this paper is based on a number of experiments in low and high speed flows in wind tunnel as well as and in-flight tests.

Skin friction measurement techniques

A number of skin friction measurement techniques exist, which can be divided into direct and indirect measurement methods. Into these groups, they also differentiate into electro-thermal -, pressure-, and mechanical methods. Some of them can be applied on wings and airfoils, but some can only be used in wind tunnel tests as reference device, like the skin friction balance.

For this purpose simultaneous skin friction measurements were made on a flat plate or wind tunnel wall, Fig. 2, in order to get a comparison between the techniques investigated.

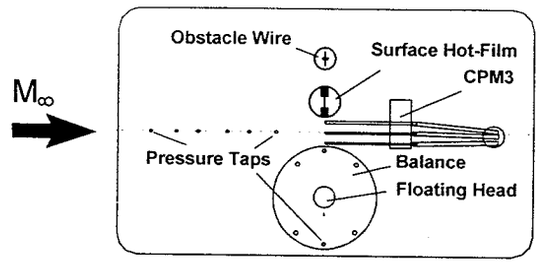

Figure 2 : Experimental set up for skin friction measurements

Methods

Skin friction balance: As a direct skin friction measurement method, the floating element balance (SM251) of Selem Inc.[3] which is designed for high speed flows[4], represents a reference device for measurements in compressible boundary layers, Fig. 3. The principle of operation of the balance is the direct measurement of the wall shear force acting on the floating element. Therefore the output voltage of the balance servo motor can be set proportional to the force (1mV = 1 mg) in positive as well as in negative flow direction, which makes measurements even in reversed flow possible.

However, in view of using the balance on airfoils, its application presents, due to its size, a rather large effort when integrating it to a wing. In case of wind tunnel models, its integration is quite impossible. Therefore the present comparative investigations were done on flat surfaces.

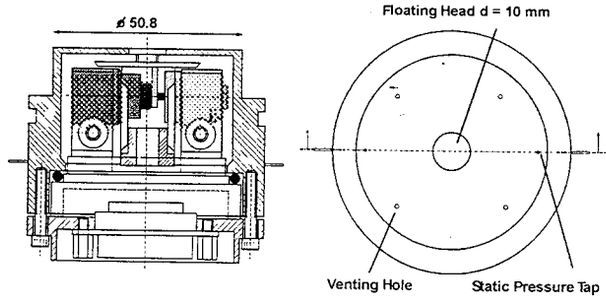

Figure 3: Floating Head Balance (SM251) for transonic flow

Computational Preston Tube Method (CPM3): The Computational Preston tube method[5] belongs to the indirect skin friction measurement techniques, however this technique needs no calibration. Here three Preston tubes of different diameter ($0.4 < d_p$ [mm] < 1.2) have to be placed directly on the wall, next to a static pressure tap, Fig. 4.

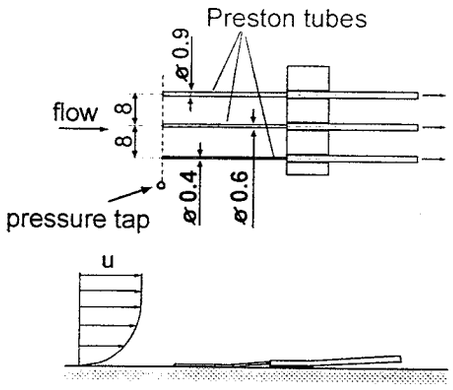

FIGURE 4: CPM3 probe for transonic tests

The measurement quantity is the dynamic pressure of each tube. On the assumption that the measured pressures can be correlated to three velocities ($u_{p,i}$; i = 1,2,3) at characteristic distances $y_{eff,i} = k_i \cdot d_{p,i}/2$ from the wall, the skin friction can be derived via a boundary layer law. The displacement factor k_i,($k_i \approx 1.3$ for turb. flow) which takes the displacement effect into account, can be described using the following empirical function of $k_i = f(u_\tau d_{p,i}/\nu)$[4]. With the CPM-code which comprises the extended van Driest boundary layer law .

$$u^+ = \int_0^{y^+} \frac{2\cdot\left(1+p^+y^+\right)dy^+}{1+\sqrt{\left[1+4\left(K_1\cdot y^+\right)^2\left(1+p^+y^+\right)\left(1-e^{-y^+\sqrt{1+p^+y^+}/A^+}\right)^2\right]}} \qquad (1)$$

$$p^+ = \frac{\nu_w}{\rho_w \cdot u_\tau^3}\cdot\frac{dp}{dx} \; ; \; A^+=26 \; ; \; K_1 = 0.4 \, .$$

a near wall velocity distribution is determined iteratively by varying the parameter K_1, starting with the standard value K_1=0.4 (von Karman constant) for turbulent flow. Eq.(1) takes the non-dimensional pressure gradient p^+ directly into account, which has to be considered in boundary layers with p.g..
When all three calculated velocities (u_{p1}, u_{p2}, u_{p3}) matches one unique velocity profile, the iteration process ends, when $\Sigma\Delta\tau_{w,i}$ is minimal.

Obstacle wire: The obstacle wire technique[7] belongs also to the indirect skin friction measurement methods and needs an individual calibration. It combines the advantage of the Preston tube and the sublayer fence, where the obstacle (a wire of known width; d_{ow} = 0.1....0.5mm) is located between two pressure taps, Fig. 5. The pressure loss Δp_{ow}, due to the obstacle can be referred to a near wall velocity u_{ow} at a height of $y_{ow}=d_{ow}/2$. Using the near wall similarity law (viscous sublayer), a correlation between the differential pressure and the skin friction, obtained by a calibration device, is as follows

$$\tau_{ow}^+ = A_{ow}\cdot\left(\Delta p_{ow}^+\right)^n \qquad (2)$$

$$\tau_{ow}^+ = \frac{\tau_w \cdot d_{ow}^2}{4\cdot\rho_w\cdot\nu_w^2} \qquad \Delta p_{ow}^+ = \frac{\Delta p_{ow}\cdot d_{ow}^2}{4\cdot\rho_w\cdot\nu_w^2} \, .$$

In order to get this empirical correlation between the non-dimensional wall shear stress τ_{ow}^+ and the non dimensional pressure difference Δp_{ow}^+, the calibration constants A_{ow}, n have to be determined using a reference.
In general, a skin friction measurement with an obstacle wire doesn't need large technical requirements. It can be used on flat walls and on curved walls like airfoils, as long as a calibration device can be applied.

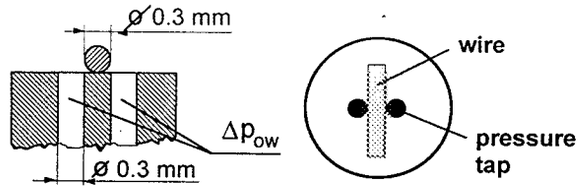

FIGURE 5: Obstacle Wire sensor

Surface Hot-film Sensors: The surface hot film, Fig. 6, is one of the indirect skin friction measurement techniques[8]. Because of the minimised sensor thickness, the film can be glued on any complex surfaces without disturbing the boundary layer. The physical principle is the analogy between the convective heat loss of a flush mounted sensor and the skin friction, keeping the element (sensor) at a constant temperature (CTA). In order to calibrate the sensor in a turbulent flow, the total heat loss is correlated to the skin friction at the wall, where the total heat loss is determined by the electrical power input to the sensor, with

$$\frac{Q_{hf}}{T_s - T_f} = A_{hf} + B_{hf}\cdot\left(\rho_{hf}\cdot\mu_{hf}\cdot\tau_w\right)^{\frac{1}{3}} \, . \qquad (3)$$

The calibration constants A_{hf}, B_{hf} can be derived using a reference device.

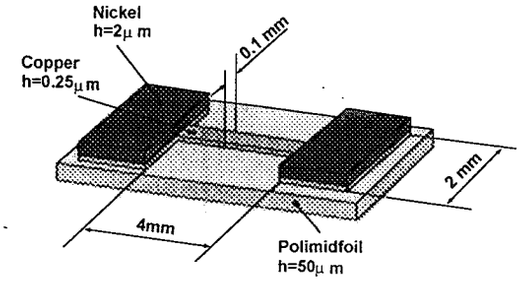

FIGURE 6: Surface Hot-Film sensor

Results

Turbulent flow: To investigate the applicability and the precision of the skin friction techniques mentioned above, measurements were carried out in an incompressible and compressible boundary layer. In Fig. 7, results of a measurement in a turbulent transonic b.l. are shown[9]. Over a wide range of Mach numbers all data of the investigated techniques present a good agreement to the theory (v. Driest II). Because of the effect of compressibility, the density as well as the viscosity change was taken into account in the calibrations.

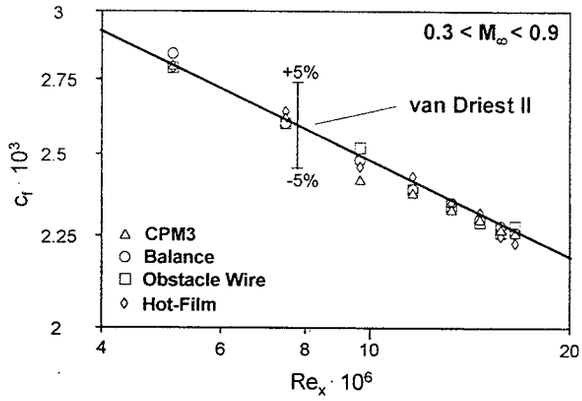

FIGURE 7: Skin friction coefficient versus local Reynolds number for a turbulent compressible boundary layer (fixed transition)

Transition: Regarding the case of b.l. transition, the location of transition is often of great interest. In this flow case, the investigated skin friction methods show again a very good agreement in the laminar, transitional and turbulent flow region without any restriction, Fig. 8.
During most of the in-flight tests a simple indication of the boundary layer state is desirable, in order to get a first on-line localisation of the transition. For this purpose, the CPM3 offers in addition to the local skin friction the possibility of calculating the b.l. shape factor. This can be done calculating the velocity profile up to u_∞ by using the CPM3-code, leading to the displacement and the momentum loss thickness and thus to the shape factor (H_{12}). In Fig. 8 the calculated shape factors in the course of transition are plotted versus the Reynolds number, showing the typical value of $H_{12}\approx 3$ for the laminar and $H_{12}\approx 1.4$ for the turbulent b.l.. Thus, an easy localisation the b.l. state is possible.

Separation: In flows with separation the use of an obstacle wire and hot-film sensors needs a backward as well as a forward calibration, which can be caused by an uneven production of the probes. Here, the obstacle wire can be used as flow direction indicator, while the hot-film only gives

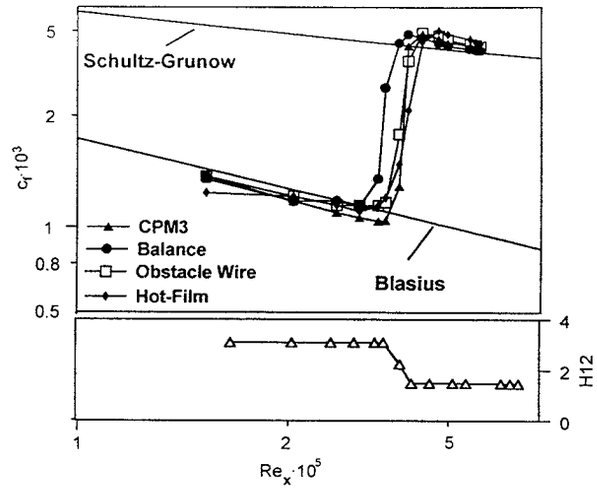

FIGURE 8: Skin friction coefficient versus Reynolds number and shape factors (derived by CPM3) in an in compressible flat plate boundary layer (low speed M< 0.1)

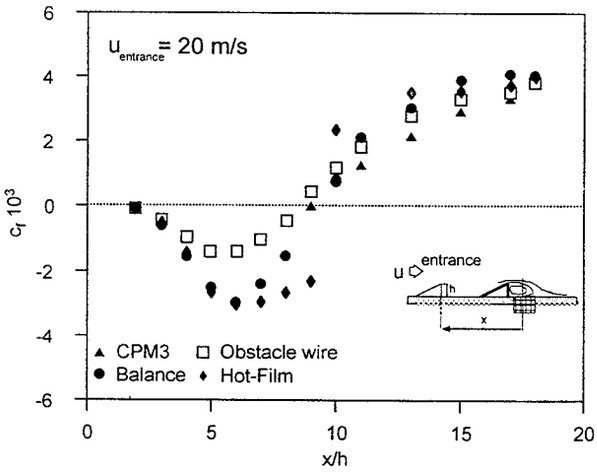

FIGURE 9: Skin friction distribution behind a step (h = 10mm) in an incompressible turbulent boundary layer

an absolute quantity. A limited use can be found in case of the Preston tubes, which are not applicable in reversed flow, without turning the probe. Fig. 9 shows the skin friction distribution behind a backward facing step in a incompressible turbulent boundary layer. From this it can be seen that the characteristic behaviour of the separation bubble including the reattachment point is indicated by all of the methods.
However, the absolute skin friction in the separation region differs considerably, which is due to the strong equilibrium b.l.. A rather good agreement of the techniques can only be found down stream of the reattachment.

Shock b.l. Interference: A slightly different behaviour was found in a transonic shock regime, where the shock was induced by shifting a displacement body, Fig. 10.

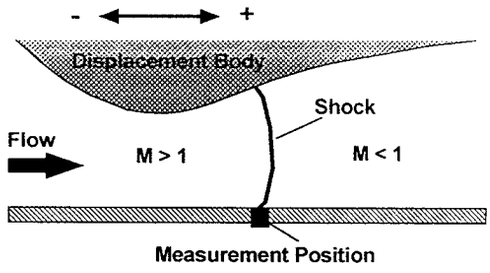

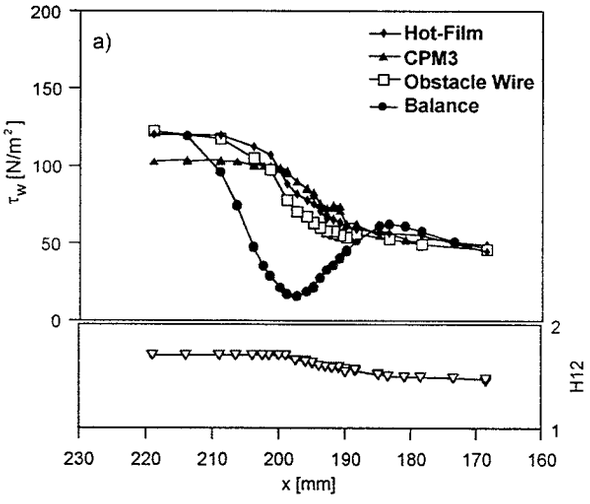

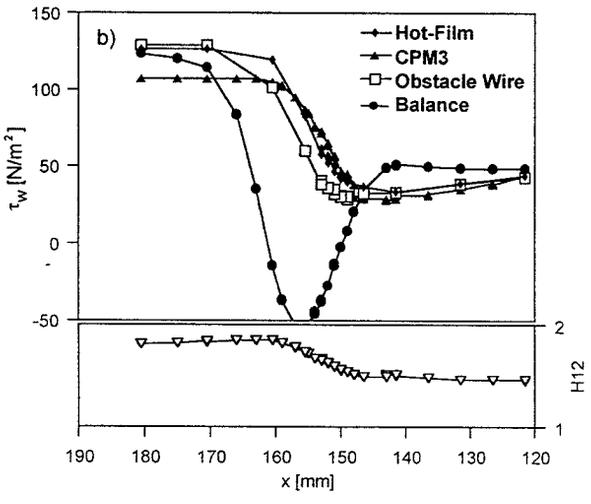

FIGURE 10: Skin friction measurement in a shock region

Here the strength of the shock seems to have a significant influence on the balance readings. In case of the weak shock, Fig. 10a, the balance shows a decrease of skin friction in the region of strong positive pressure gradients. A similar behaviour can be found in the strong shock test case, Fig. 10b, where the indicated skin friction values of the balance are below zero. However, this flow separation is not confirmed by the results of the other skin friction techniques.

With the pressure gradient correction of the obstacle wire and the hot film[9], the results show no large deviation to each other, except directly in the shock region. The CPM3 shows a decrease in τ_w at 180 < x [mm] < 160 where the shock effect in front of the probe causes a reduction of the measured dynamic pressure. This is due to erroneous reading (location) of the static pressure tap which is not taken into account yet. Again, calculating the shape factor out of the Preston tube data, the region upstream and downstream the shock is indicated clearly, where the region of M < 1 with H_{12}=1.4 represents the turbulent flow case.

Flight test: To give an example of the application of one of the skin friction techniques mentioned in this paper, a CPM3 probe was used on a A320 in-flight test. Therefore the probe was applied on the 'upper' fin surface in order to control whether the b.l. is turbulent in any flight condition investigated. The results are shown in Fig. 11, where the skin friction coefficients are plotted versus the Reynolds number. The Mach number of 0.43 < M_∞ < 0.73 was changed due to the variation of the angle of attack. The results compare well with the van Driest II theory, giving a good account of the compressible turbulent flow over the fin.

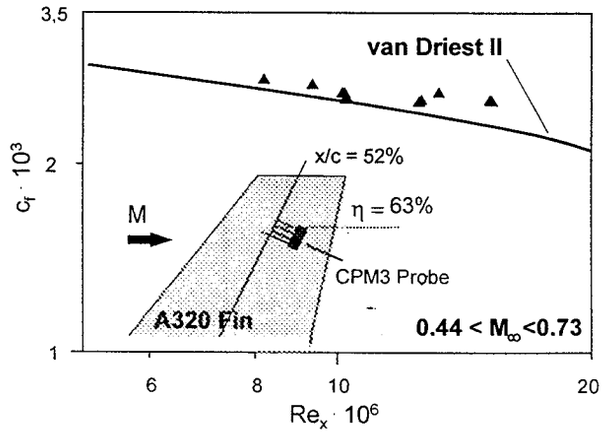

Figure 11: Results of CPM3 measurements an a fin of the A320 in-flight test

Array surface measurements

Methods

Hot-film arrays: A hot film array consists of a number of one behind each other arranged sensors, Fig. 12 . The calibration of in-line hot-film arrays is important, in case of investigating the skin friction distribution on bodies. Here, the temperature wake induced by upstream surface hot-films as well as the structural coupling of the sensors becomes increasingly important for

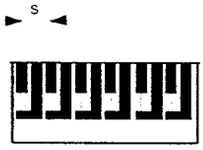

Figure 12: Surface hot-film array

calibration[10]. Because of this, conventional single sensor calibration cannot be applied automatically for multi sensor arrays.

Piezofoil Sensors and Sensor-Arrays: A single piezofoil sensor, Fig. 13a can be considered as a plate capacitor with a very low capacity and mass. Thus, because of to the inherent loss of capacity over time, it is only possible to measure dynamically. Charge fluctuations can be caused by pressure fluctuations normal to the wall or shear stress fluctuations tangential to the wall (depending on the preferred orientation of the polymer molecules due to the mechanical stretching) as well as by temperature fluctuations in the near wall flow field, Fig. 13b. The sensor signals can be amplified by means of simple charge amplifiers. The possible frequency range of this kind of sensors is only limited by the lower limiting frequency of the employed charge amplifiers (typically 1.6 to 160 Hz) and its own resonance frequency (up to 10^9 Hz). An improvement of the piezofoil measurement technique was obtained by using a small temperature gradient between sensor and fluid to
obtain higher signal amplitudes and thus, signal-to-noise ratios [11]. Since pressure fluctuations as well as temperature or shear stress fluctuations are both correlated with near wall velocity fluctuations u' in boundary layers, the use of the pyroelectric properties is a good means to receive qualitative measurements of surface force fluctuations.

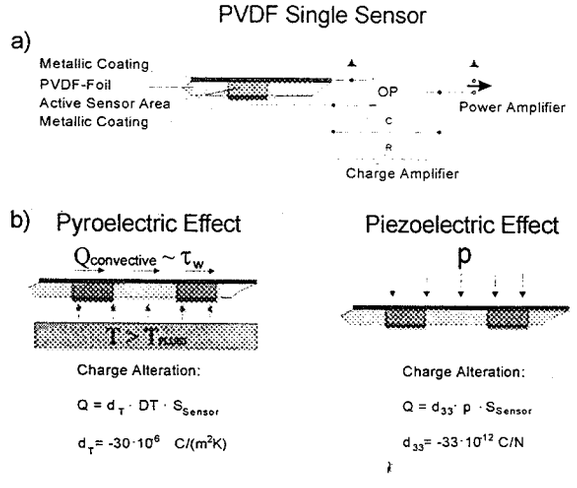

FIGURE 13: Schematic sketch of a piezofoil sensor

Liquid Crystals: The liquid crystal foil consists of encapsulated liquid crystals, which are sensitive to temperature changes on the surface[12],[13],[14]. Due to this the temperature variation in the b.l., which is also an indication of the actual b.l. state, can be monitored by the foil changing its colour. This allows an easy and distributed visualisation of the wall flow.
In order to get the temperature image of the liquid crystal foil, only a simple CCD-camera is needed. The resolution of the foil, which is quite important for the quality of the results, depends on the underlying substrate, which is responsible for a lower temporal resolution and the size of the crystal balls, determining the spatial resolution.

Results

Thermal interaction:
According to Fig. 14, the heat loss of a surface hot-film will be affected by neighbouring sensors.
However, this will be influenced by the spacing of the sensors, i.e. the ratio of sensor spacing to effective sensor length s/L_{eff} is an important parameter. Strong thermal interaction will appear if the spacing is almost similar to the effective sensor length L_{eff}, thus $s/L_{eff} \approx 1$. This effect of the thermal interaction via structure and flow will mainly influence the downstream sensor. Furthermore, regarding the spherical temperature distribution in the substrate material below a surface hot-film, one can assume that the relation between relative heat loss change of the downstream sensor and the sensor spacing will be anti-proportional, i.e. $\Delta Q_{el} \sim 1/s$ or $\Delta \tau_w[\%] \approx 1/s$. As an example, Fig. 15 shows the resulting heat loss changes of an in-line array due to the thermal interference as a function of the viscous hot-film length. Parameters are the number of upstream operated sensors, Fig. 15a, and the sensor spacing, Fig. 15b. As a result obtained from these investigation, Fig 14a shows that the relative heat loss in terms of $\Delta Q_{el}/Q_{el,ref}$ increases asymptotically with the number of sensors operated upstream of the sensor considered. On the other hand, the measurement error decreases with increased spacing of the sensors, see Fig. 15b. The measurement error in

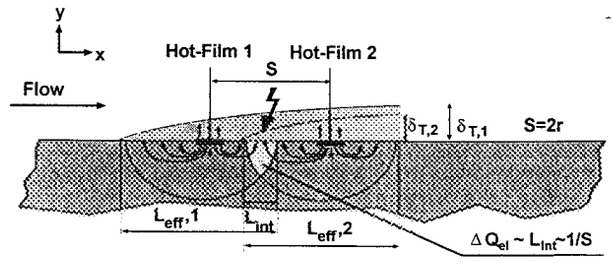

FIGURE 14: Principle sketch of the thermal interference between two surface hot film sensors

terms $\Delta\tau_w$ [%] depends on the individual sensitivity of the hot-film considered, and varies from 3% up to 22%. Furthermore, it can be seen from the figure that the change of the relative heat loss of a hot-film sensor caused by an upstream operated sensor is - in case of turbulent flow - a function of the wall shear stress itself. Based on the experimental results, a standard calibration procedure was derived, estimating the influence of the thermal interaction in a wide range of wall shear stress by only a few measurement points. This standard calibration procedure is based on similarity parameters, predominately on the viscous length of the hot-film and is depicted in Fig.15 (lines), this standard calibration for in-line hot-film arrays can be written as follows:

$$\frac{\Delta Q_{el} / Q_{el,ref}}{\sqrt{N_s} / (s / l_s)} = A + B \cdot l_s^{+\,-1/3} \qquad (4)$$

and - in turn - can be used to derive a minimum distance for the streamwise spacing of hot-film sensors. Furthermore, taking into account the effect of the thermal conductivity of the wall:

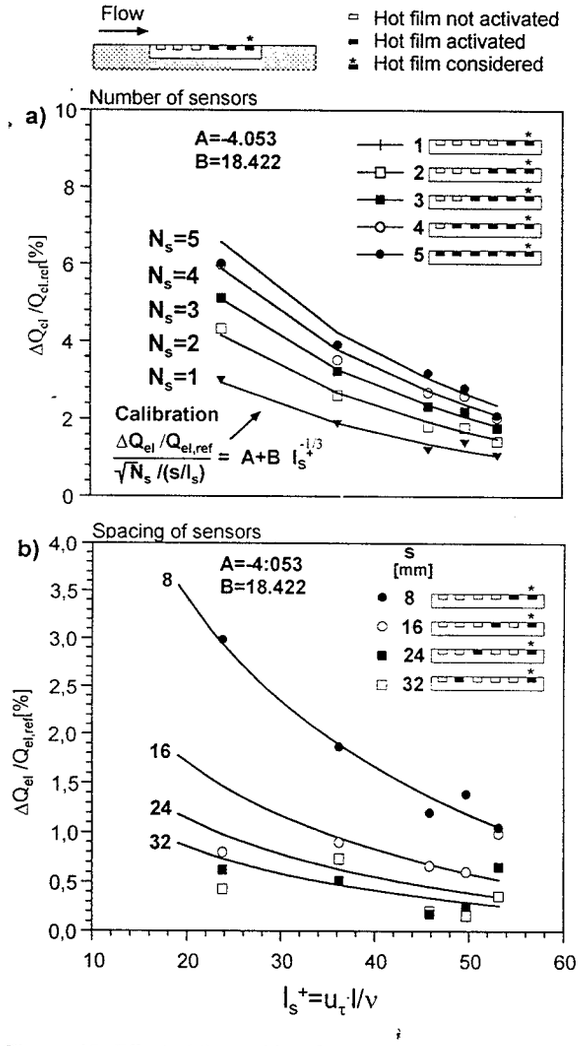

Figure 15: Effect of thermal interference on the calibration of a hot-film sensor out of an in-line hot-film array a.) no. of sensors operated upstream, b.) spacing of sensors

$$\frac{\Delta Q_{el} / Q_{el,ref}}{\sqrt{N_s}} = A \cdot \lambda_{Substrate}^{\;-2/3} \qquad (5)$$

it is possible to derive design rules for the layout of in-line hot-film arrays which are suitable for different wall shear stress regimes and wall materials.

Transition on airfoils: For recent measurements with a laminar wing glove a piezofoil array with 192 individual sensors was employed. This array was used for in-flight as well as wind tunnel experiments concerning the development of an artificially induced disturbance wave emanating from a harmonic point source (3D-excitation)[15]. The sensors on this array were arranged in a rectangular pattern with a grid size of 6 by 6 mm and covered the region from x/c=0.40 to x/c=0.48 of the employed airfoil glove. The spanwise extension was 54 mm, equal to y/c=0.04, Fig 16.
The wind tunnel and flight tests were carried out with different excitation frequencies at a Reynolds number of 3.0 x 10^6. As a first result, the distribution of RMS-values from the centreline sensors are shown in Fig 17. Here, the high RMS-values mark the transition position. The signals are filtered through a bandpass (f_E +/- 0.1 f_E) only to show the development of the excitation frequency. Without artificial excitation, the transition was located downstream from x/c=0.48. With artificial excitation, transition moves upstream. The most unstable frequency (in this case f_E=900 Hz) causes the most upstream transition position. This is in very good agreement with the linear stability theory. A similar effect can be seen in Fig 18, which shows results obtained in flight tests employing the same test set up. The distribution of relative RMS-values, Fig. 18a, for the three excitation frequencies 700 Hz, 900 Hz and 1100 Hz shows again the upstream travelling of transition due to excitation frequencies close to the natural instability frequency f_E=900Hz. The bandpass filtered RMS-values, Fig. 18b, employing the same test behaviour.

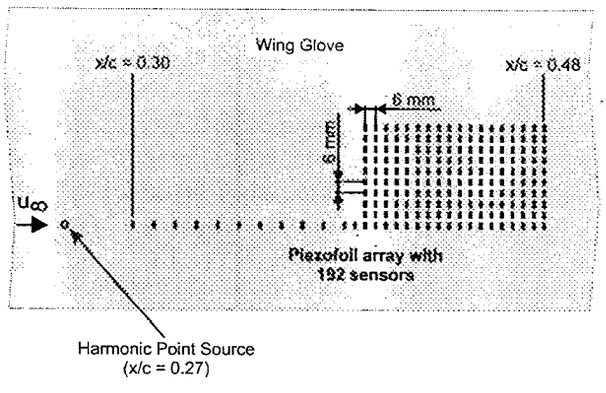

FIGURE 16: Layout of 192-sensor array for flight tests

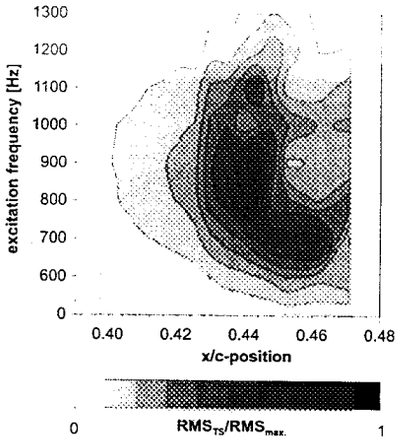

FIGURE 17: Transition position due to different excitation frequencies (wind tunnel test)

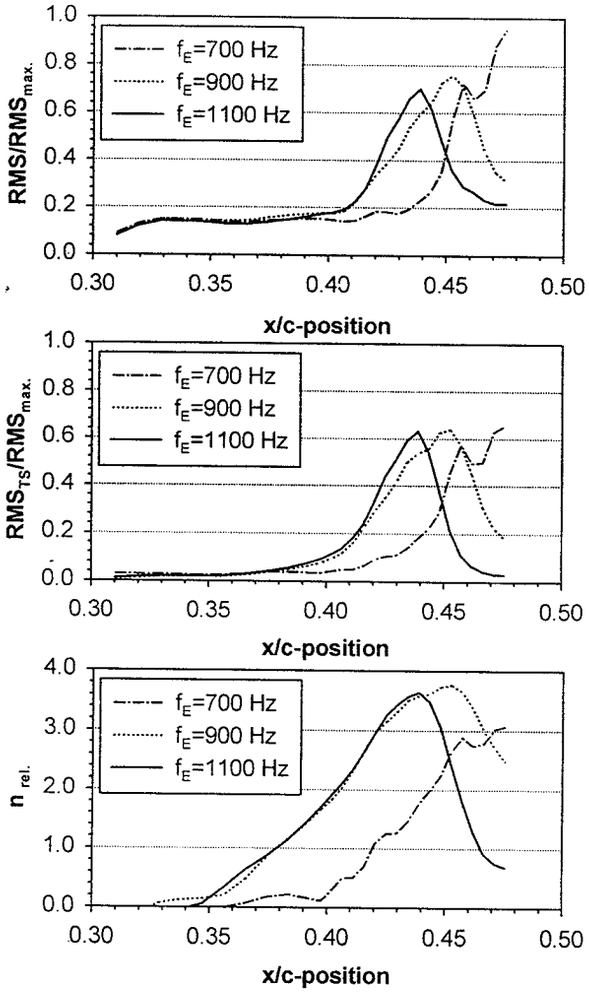

FIGURE 18: RMS-values, RMS$_{TS}$-values and relative n-factors for different excitation frequencies (flight test)

The comparison of the unfiltered with the filtered RMS-values shows that the artificially excited frequency is responsible for about 90% of overall signal strength for the frequencies close to the natural instability frequency. Since the signal

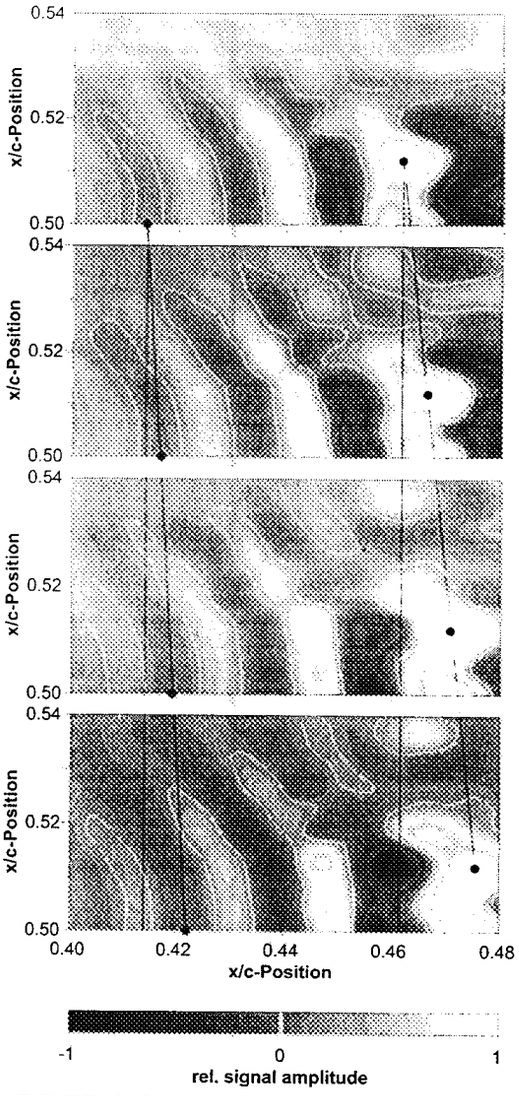

FIGURE 19: Snapshots of instantaneous sensor amplitudes due to artificial excitation (f_E=700 Hz, flight test)

amplitude at the point of neutral stability, which is necessary for the determination of n-factors according to the classical e^N-method, is not known from these experiments, only relative n-factors

$$n_{rel.} = \ln\left(\frac{A_x}{A_{min}}\right) \qquad (6)$$

with A_x :sensor amplitude
$A_{min.}$: min. sensor amplitude

could be calculated from the sensor signals for different excitation frequencies. (lower diagram). Waves with frequencies close to the natural instability frequency (in this case f_E= 900 Hz and 1100 Hz) show an increase in signal strength almost immediately downstream from the point source. Lower frequencies are initially dampened and show this increase further downstream which, also in good agreement with the linear stability theory.

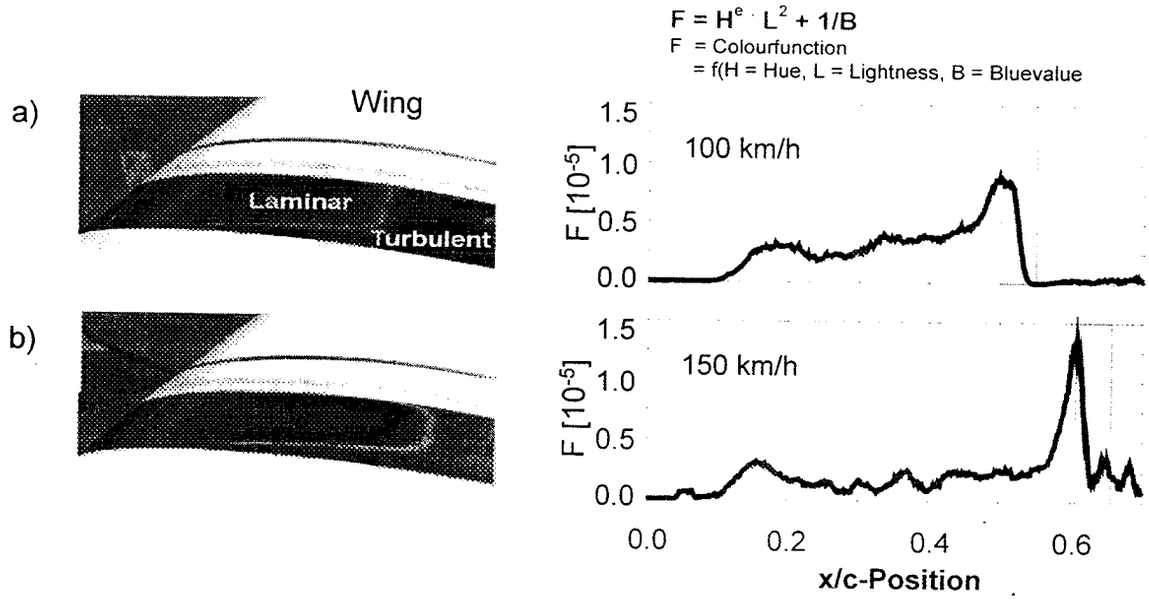

FIGURE 20: Visualisation of the transition on a laminar wing in a flight test (left: video image, right: resulting colour value from digital image analysis), a) 100 kph and b) 150 kph

A more detailed analysis of the wave patterns in the boundary layer due to artificial excitation (f_E=700 Hz) is shown in Figure 19. Here, four snapshots of instantaneous signal amplitudes with a delay of 0.2 ms between each other are depicted, showing the temporal development of the excitation wave. The characteristically half moon shaped patterns on the left hand side of the observed regions become perturbed by oblique waves, which lead to strong spanwise changes in signal amplitude. The acceleration of the wave velocity during transition can be seen following the marked lines in Fig. 19.

As a further example, some experimental results from wind tunnel and flight investigation shall give an outline of the capabilities of liquid crystals in monitoring transition. Here, a wing glove equipped with a heated liquid crystal foil (0.4 x 1.2m) was used in a flight test, investigating the laminar-turbulent transition on a laminar wing. Exemplary results of this are shown in Fig. 20a and b, were the transition is clearly indicated by the white line in the images, moving downstream with increasing speed and decreasing angle of attack.

The corresponding results of the digital image processing are shown on the right hand side of the figure. Here, the strong decrease in the colour function value indicates the transition position.

Furthermore, a swept wing was investigated in a wind tunnel under transonic flow conditions. Fig. 21 shows the transitional swept wing flow monitored by liquid crystals on its surface at M_∞=0.7. From this the typical shape of a cross flow transition (distance of streaks s=4.2mm $\approx 6\cdot\delta$) can be seen and the different boundary layer states whether laminar, transitional or turbulent can easily be taken from the different colour or shading.

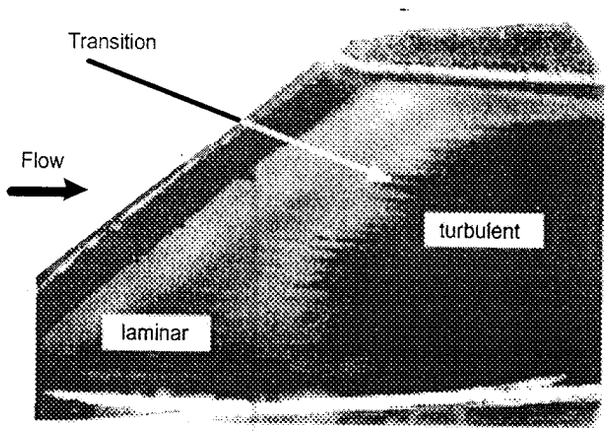

FIGURE 21: Visualisation of the transition due to cross flow on a swept laminar wing (M=0.7) by means of liquid crystals for α=-2° (wind tunnel test)

Conclusions

The main subject of the present paper are actual comparative investigations of different surface measurement techniques, with respect to wind tunnel and in-flight tests. The basic aim was to investigate the capability of surface sensors in subsonic and transonic flows, including flow transition, shock b.l. interaction and separation.
Regarding the application of the investigated wall shear stress measurement techniques it is shown that from hot-film sensors and obstacle wires quantitative information about the skin friction can be obtained, except in separated flows. In case of a densely packed hot-film array the influence of the sensor spacing has to be taken into account resulting in a standard calibration. This leads to a reduction of the flow field dispersal due to the minimum sensor spacing. In contrast to that, the Computational Preston Tube Method offers a rather good possibility to achieve quantitative (τ_w) as well as qualitative (H_{12}) results in order to get an actual and immediate information about the boundary layer state, which can be very important during in-flight tests as well as in flight operations. Multi sensor piezofoil arrays for the qualitative measurement of surface force fluctuations were employed successfully for measurements in transitional boundary layers subject to an artificial excitation in wind tunnel as well as in flight tests. The piezofoil technique allows measurements with high spatial and temporal resolutions.
For a wide range of flow velocities the liquid crystal foil provides a simple technique to visualise boundary layer states in large flow areas. Using the surface temperature changes within a flow regime, flow phenomena as the laminar, transitional and turbulent boundary layer state can be detected. In order to compare the relative merits of the measurement techniques investigated, Table 1 gives an overview of their individual capabilities and possible applications on b.l. phenomena in subsonic and transonic airfoil flows.

	Quantity	W.T.	In-Flight	ADIW	Cal.	τ' , p'	Ts.	Sep.	F.D.	Sh.	Appl	E.Ef.
f. e. Balance	$\pm \tau_w$	+	--	--	--	q.s.	+	+	+	+	r	h
CPM3 probe	τ_w , H_{12}	+	+	+	--	q.s.	+	--	--	+	e	l
Obstacle Wire	$\pm \tau_w$	+	+	+	+	q.s.	+	+	+	+	e	l
Surface Hot-Film (Array)	τ_w , τ_w'	+	+	+	+	h, < 50kHz	+	--	--	+	d	h
LCF	T_w (q_w)	+	+	+	+	q.s.	+	+	--	+	d	l
Piezofoil	p', τ_w'	+	+	+	--	h up to 1Ghz	+	+	--	+	d	h

W.T. -Wind Tunnel ; **ADIW** - Adaptive Wing ; **Cal.** - Calibration; **Ts.** - Transition; **Sep.** - Separation; **F.D.** - Flow Direction; **Sh.** - Shock; **Appl.** - Application; **E.Ef.** - Experimental Effort; **h** - high; **+** - yes; -- - no; **r** - restricted; **e** - easy; **q.s.** - quasi static; **d** - difficult; **l** -low

Table 1: Relative merits of surface measurement techniques

References

[1] W.Nitsche, J.Szodruch, 1993, „Laminar flow instrumentation for wind tunnel and flight experiments", Journal of Aircraft, Vol.30, No.2, pp.192-200

[2] B.Ewald, F.Durst, E.Krause, W.Nitsche, 1993, „In-flight measuring techniques for laminar flow wing development", Zeit. Flugwiss. Weltraumforschung, Vol.17, pp.294-310

[3] V.D.Nguyen et al, 1984, „The determination of turbulent skin friction behind a flat plate turbulence manipulators using servo-controlled balances", ICAS-84-2.4.2

[4] L.C.Squire, A.M. Savill,1996, „Experimental results on airfoil manipulators at high subsonic speeds", Exp. In Fluids No. 21, pp.275-285

[5] W.Nitsche, R.Thünker, C.Haberland, 1983, „A computational Preston tube Method", Turb. Shear Flows 4, Springer Verlag, pp.261-275

[6] W.P.Joeng, S.H.Kang, 1995, „Measurements of transitional boundary layer on a flat plate using a computational Preston tube method", Exp. Fluids 20, pp. 29-37

[7] N.Weiser, W.Nitsche, F.Renken, 1991, „Wall shear stress determination by means of obstacle wires", Proc. of 8th Symp. of Turb. Shear Flows, pp. 4-5-1 - 4-5-6

[8] F. Haselbach, W.Nitsche, 1996, „Calibration of single-surface hot-films and in-line hot-film arrays in laminar or turbulent flows", Meas. Sci. Technol. 7, pp.1428-1438

[9] S.Bose, F.Haselbach, T.Ehlers, W.Nitsche, 1997,"Comparative investigations on the reliability of direct and indirect skin friction measurement techniques in compressible flow", Proc. 5th FLUCOME, Vol. 1, pp.107 - 113

[10] F.Haselbach, 1997, „Thermalhaushalt und Kalibration von Oberflächenheißfilmen und Heißfilmarrays", PhD Thesis, TU Berlin, VDI-Verlag Reihe:7, Strömungstechnik, Nr.326

[11] Kawai, H., 1969, "The piezoelectricity of poly-vinyliden fluoride", Jpn. J. Appl. Phys. 8, pp. 975-976

[12] Gall, P.D., Holmes, B.K., 1986, „Liquid crystals for high altitude in-flight boundary layer flow visualization", AIAA-paper 86-2592

[13] Hoang, Q.H., Toy, N., Savory, E., 1995, „Liquid crystals for surface shear stress measurements", Proc. of the 7th Intern. Symposium on Flow Visualization, Sept. 11.-14., Seattle, USA, pp. 552-557

[14] Kasagi, N., Moffat, R.J., Hirata, M., 1989, „Liquid crystals", Handbook of Flow Visualization, Chapter 8, Ed. W.J. Yang, Hemisphere Publ. corp.

[15] J.Suttan „Design and tests of a PVDF array with high spatial resolution for unsteady surface force measurements in a transitional boundary layer.", PhD thesis, TU Berlin, to be published